Journal of Biomedical Optics

BiomedicalOptics.SPIEDigitalLibrary.org

Diagnosis of malignant pleural mesothelioma from pleural fluid by Fourier transform-infrared spectroscopy coupled with chemometrics

Sherif Abbas
Nihal Simsek Ozek
Salih Emri
Deniz Koksal
Mete Severcan
Feride Severcan

Sherif Abbas, Nihal Simsek Ozek, Salih Emri, Deniz Koksal, Mete Severcan, Feride Severcan, "Diagnosis of malignant pleural mesothelioma from pleural fluid by Fourier transform-infrared spectroscopy coupled with chemometrics," *J. Biomed. Opt.* **23**(10), 105003 (2018), doi: 10.1117/1.JBO.23.10.105003.

Journal of Biomedical Optics 23(10), 105003 (October 2018)

Diagnosis of malignant pleural mesothelioma from pleural fluid by Fourier transform-infrared spectroscopy coupled with chemometrics

Sherif Abbas,[a,b,†] Nihal Simsek Ozek,[a,c,d,†] Salih Emri,[e,f,*] Deniz Koksal,[e] Mete Severcan,[g] and Feride Severcan[a,h,i,*]
[a]Middle East Technical University, Department of Biological Sciences, Ankara, Turkey
[b]Ain Shams University, Physics Department, Cairo, Egypt
[c]Ataturk University, Department of Biology, Erzurum, Turkey
[d]Ataturk University, East Anatolian High Technology Research and Application Center (DAYTAM), Erzurum, Turkey
[e]Hacettepe University, Department of Chest Diseases, Ankara, Turkey
[f]Altinbas University, Department of Chest Diseases, Faculty of Medicine, Istanbul, Turkey
[g]Middle East Technical University, Department of Electrical and Electronic Engineering, Ankara, Turkey
[h]Altinbas University, Department of Biophysics, Faculty of Medicine, Istanbul, Turkey
[i]Altinbas University, Graduate Program of Biomedical Sciences, Institute of Health Sciences, Istanbul, Turkey

Abstract. This study was conducted to differentiate malignant pleural mesothelioma (MPM) from lung cancer (LC) and benign pleural effusion (BPE) from pleural fluids using the diagnostic power of Fourier transform-infrared spectroscopy with attenuated total reflectance mode coupled with chemometrics. Infrared spectra of MPM ($n = 24$), LC ($n = 20$), and BPE ($n = 25$) were collected, and hierarchical cluster analysis (HCA) and principal component analysis (PCA) were applied to their spectra. HCA results indicated that MPM was differentiated from LC with 100% sensitivity and 100% specificity and from BPE, with 100% sensitivity and 88% specificity, which were also confirmed by PCA score plots. PCA loading plots indicated that these separations originated mainly from lipids, proteins, and nucleic acids-related spectral bands. There was significantly higher lipid, protein, nucleic acid, and glucose contents in the MPM and LC. However, the significant changes in triglyceride and cholesterol ester content, protein and nucleic acid structure, a lower membrane fluidity, and higher membrane order were only observed in the MPM. To check the classification success of some test samples/each group, soft independent modeling of class analogies was performed and 96.2% overall classification success was obtained. This approach can provide a rapid and inexpensive methodology for the efficient differentiation of MPM from other pleural effusions. [DOI: 10.1117/1.JBO.23.10.105003]

Keywords: pleural fluid; malignant pleural mesothelioma; lung cancer; Fourier transform-infrared spectroscopy; chemometrics; benign pleural effusion.

Paper 170679RR received Oct. 18, 2017; accepted for publication Sep. 13, 2018; published online Oct. 13, 2018; corrected Oct. 16, 2018.

1 Introduction

Malignant pleural mesothelioma (MPM) is a highly aggressive, incurable malignancy originating from the mesothelial cells lining the pleural cavity.[1,2] It is mainly caused by occupational or environmental exposure to asbestos and erionite.[3,4] Due to its long latent period, its incidence will continue to increase during the next two decades worldwide especially in industrialized countries.[5,6]

The initial diagnosis/evaluation of MPM is based on the use of noninvasive imaging methods such as ultrasonography, computerized tomography (CT), and magnetic resonance imaging (MRI). To confirm the diagnosis, pathological assessment of pleural fluid and biopsy samples is required.[7] However, the cytological diagnosis of MPM on a pleural effusion is prone to error due to inadequate specimens. Moreover, obtaining biopsy samples during thoracoscopy is an invasive procedure and patients often refuse it or physicians postpone this procedure, resulting in significant delays in diagnosis.[7,8] Due to the mentioned disadvantages of the current diagnostic methods, the diagnosis of MPM is really challenging. Furthermore, the confirmation of its diagnosis is prolonged due to difficulty in distinguishing MPM from lung cancer and benign pleural effusions (BPEs), which causes poor prognosis, a high mortality and morbidity. To decrease morbidity and improve survival of MPM, new diagnostic approaches which are accurate, minimally invasive, rapid, low-cost, operator-independent, and capable of generating reliable information, are urgently needed. Recent studies indicated that Fourier transform-infrared (FTIR) spectroscopy coupled with chemometric approach has the ability to diagnose different cancer types such as lung, prostate, bladder, and ovarian cancer,[9–15] since this technique enables to elucidate disease-induced alterations in molecules by performing qualitative and quantitative analysis on spectral bands. A recent study has indicated the efficiency of FTIR imaging in the resolving of tumor subtypes in diffuse malignant mesothelioma.[16] Our preliminary Infrared (IR) spectroscopy studies performed with a limited sample number of pleural fluid and serum of MPM, LC, and BPE patients indicated the discrimination of MPM from other two groups.[17–19] This study is going to be the first article on this subject which reveals, in addition to detailed

*Address all correspondence to: Feride Severcan; E-mail: feride.severcan@altinbas.edu.tr; Salih Emri, E-mail: salih.emri@altinbas.edu.tr

†Both authors contributed equally to this manuscript.

1083-3668/2018/$25.00 © 2018 SPIE

spectral characterization studies, succesfull differentiation of MPM and LC from a benign group and from each other using pleural fluids by ATR-FTIR spectroscopy coupled chemometric methods as a rapid, low-cost, and operator-independent technique. To identify the relative spectral differences between MPM, LC, and BPE groups and to classify them, unsupervised, namely hierarchical cluster analysis (HCA) and principal component analysis (PCA) as well as supervised, namely soft-independent modeling of class analogy (SIMCA), chemometric approaches were performed since these analysis methods enable the categorization and extraction of meaningful information from complex and large spectral datasets and enhance the diagnostic efficiency of the IR spectroscopy.[20,21]

2 Experimental Section

2.1 *Patients*

The study protocol was approved by Hacettepe University Ethics Committee (HK 12/131-36). Before collecting pleural fluid samples, a written informed consent was taken from all patients following the ethical norms of the institute. The samples were collected from patients with MPM, LC, and BPE. All the patients were treatment-naive. The characteristics of the patients are summarized in Table 1. BPE was considered as a control group since the pleural fluids of such patients were due to benign diseases, mostly congestive heart failure. MPM and LC diagnosis were confirmed by standard Hematoxylene-Eosin and immunohistochemical staining of biopsy specimens from open tumor biopsies obtained during thoracoscopy and stained as recommended by Hussain et al.[7] The diagnosis of BPE was confirmed according to light's criteria[22] via the analysis of protein and LDH levels in both pleural fluid and serum and cytologically.

2.2 *ATR-FTIR Spectroscopy*

2.2.1 *Sample preparation and spectral acquisition for FTIR spectroscopy*

Before each FTIR measurement, frozen samples were thawed at room temperature. The IR spectra of the samples were collected using one bounce attenuated total reflectance (ATR) mode on a Perkin Elmer Spectrum 100 FTIR spectrometer (Perkin Elmer Inc., Norwalk, Connecticut, USA) equipped with a universal ATR accessory. Briefly, 1 μl of pleural fluid was placed on the diamond/ZnSe crystal of ATR unit and dried with mild nitrogen gas for 3 min to remove excess unbound water. This process was repeated two more times in order to produce enough sample thickness for ATR measurement attained via a total of 3 μl of pleural fluid. Each spectral measurement was collected with 28 scans between the 4000 and 650 cm^{-1} spectral range at a resolution of 4 cm^{-1}. Since water molecules in the air affect IR spectra,[23] the spectrum of the empty diamond/ZnSe crystal was recorded as background and subtracted automatically using the appropriate software (Spectrum 100 software, Perkin Elmer). Recording and analysis of the spectral data were performed using Spectrum One software of Perkin Elmer. For each sample, three randomly taken replicates were scanned, which revealed almost identical spectra, and the spectral average of these replicates was used in further analysis. To check the reproducibility of this technique, all spectral collections were performed by two different operators at different times.

Table 1 Patient characteristics.

Groups	Age (mean ± SD) years	Gender	Diagnosis
BPE	64 ± 14.5	11 male	82% heart failure
		14 female	18% others[a]
LC	63 ± 7.7	15 male	76% adenocarcinoma
		5 Female	24% others[b]
MPM	63.5 ± 9.7	14 male	100% MPM
		10 female	

Note: BPE, benign pleural effusion; LC, lung cancer; MPM, malignant pleural mesothelioma.
[a]Premalignant effusion, postoperative effusion, acute renal failure, and chronic liver disease.
[b]Squamous cell ca, small cell ca, and adenosquamous ca.

2.2.2 *Spectral preprocessing and data analysis*

For chemometric analysis, the spectral preprocessing and manipulation operations were carried out by OPUS 6.5 software (OPUS, Bruker Optics, and Ettlingen, Germany). Raw IR spectra from all pleural fluid samples were baseline corrected using the OPUS 6.5 software function known as concave rubber band with 64 baseline points and 12 iteration points. This baseline correction method has been successfully and commonly used in other studies.[24–26] Then the spectra were vector normalized in order to remove the effect of overall scaling occurring during sample measurements.[27,28] The resulting preprocessed spectra were then used for further chemometric analysis.

For characterization studies, the quantitative spectral analyses including spectral band position, bandwidth, and band area ratio analyses were calculated from the baseline corrected averaged IR spectra using Spectrum One software (PerkinElmer Inc., Norwalk, Connecticut, USA). The spectral regions including 3800 to 2800 cm^{-1} and 1800 to 650 cm^{-1} were used for these analyses. The band position values were determined from the peak position corresponding to the center of weight from the baseline corrected spectra. The bandwidth value of CH_2 antisymmetric stretching band was measured from 0.8× height of the absorption spectra in terms of cm^{-1}. The band area ratios were calculated by calculating the ratio of the areas of the relevant bands. Although it does not give precise information, to visually demonstrate spectral variations between studied groups a min–max normalization process was performed based on amide A band.

2.2.3 *Unsupervised chemometric analysis*

HCA and PCA were performed using Unscrambler X (Camo Software, Inc.) program.

HCA enables to assess the similarity between samples by measuring the distances between their points in the space of measurement.[13] Similar samples lie close to one another, whereas dissimilar samples are distant from each other.[29] HCA was performed first, in pairs of MPM and LC groups and MPM and BPE groups in the 3300 to 2800 cm^{-1} and 1800 to 650 cm^{-1} spectral regions to check whether the spectra of each group have enough variation within each pair. Then HCA was performed for the three groups (MPM, LC, and BPE) in

Table 2 Definitions for sensitivity and specificity for HCA based on ATR-FTIR spectroscopic data.

Group	Positive[a]	Negative[a]	
MPM	A	B	Sensitivity $= A/(A+B)$
Control (BPE)/LC	C	D	Specificity $= D/(C+D)$

[a]Positive and negative values are determined as follows:
A is the number of MPM patients identified in MPM group (true positive).
B is the number of MPM patients identified in only LC or BPE groups (false negative).
C is the number of LC or BPE patients identified in MPM group (false positive).
D is the number of LC or BPE patients identified in only LC or BPE groups (true negative).

the 3300 to 2800 cm^{-1} and 1800 to 650 cm^{-1} spectral regions to check whether the spectra of each group also have enough variation between themselves. To measure the performance of the differentiation method obtained from HCA, sensitivity and specificity were calculated as described in Table 2.[30]

PCA is used to reduce the dimensionality of the data by projecting the data using a linear transformation onto a new space consisting of orthogonal vectors. The transformation matrix consists of the eigenvectors of the correlation matrix of the whole set of spectra.[31] The coordinates of the new space are the principle components (PC) and each sample is represented by a score value along each PC.[32] Each PC describes the variations among samples in decreasing order. Thus the first principle component, i.e., PC1, expresses most of the variance in the data; PC2 expresses the second largest variance in the data and so on. Most of the time, only a few PCs are sufficient to approximate the whole data. Therefore, using a two-dimensional (2-D) or three-dimensional scores plot, it is possible to visualize the whole set of samples by points in a single graph each point representing a sample. As a result, information about the class separation is obtained by clustering similar samples from the scores plot. An increase in the spatial separation between two points in a scores plot corresponds to an increase in the dissimilarity between these two samples, i.e., the absorbance spectra in the case of FTIR spectra as the input.

PCA was carried out first for the 3300 to 2800 cm^{-1} and 1800 to 650 cm^{-1} spectral regions, for the MPM-LC and MPM-BPE pairs of groups and then to the three groups (MPM-LC-BPE). To obtain more specific results, PCA was also carried out for the C—H stretching (3050 to 2800 cm^{-1}) and fingerprint (1800 to 650 cm^{-1}) spectral regions. The analyses were performed on vector normalized spectra that were 11 points smoothed with the Savitzky–Golay algorithm. PCA was implemented using "The Unscrambler X" software Version 10.3. Nonlinear iterative partial least squares algorithm was used with full cross validation.

2.2.4 *Supervised chemometric analysis*

SIMCA was carried out for the 3300 to 2800 cm^{-1} and 1800 to 650 cm^{-1} spectral regions using Unscrambler X (CAMO Software, Inc.) program. SIMCA is a PCA-based supervised chemometric approach. At first, PCA was carried out for the whole data set in order to identify different classes of observations and for each class a PCA model was obtained. Then new samples were tested with each class model to see how similar they are to the tested class model.[33]

First, three samples from each group are randomly removed to be used as blind test samples. Then using the new groups, PCA models for each group were created and these models are tested with the blind samples. This process was repeated 10 times and the average accuracy value was calculated.

2.3 *Statistical Analysis*

All spectral results of MPM, LC, and BPE groups were expressed as mean ± standard error of mean. First, all data were analyzed by Kolmogorov–Smirnov tests to see whether or not they are normally distributed. Then they were statistically compared using one-way ANOVA, and furthermore Dunnett's test was used for the comparison of the studied groups in a pairwise manner (GraphPad Prism 6.01 (GraphPad Software, Inc.). A "p" value ≤ 0.05 was considered as statistically significant. The degree of significance was denoted as less than or equal to $p < 0.05$*, $p < 0.01$**, $p < 0.001$***, and $p < 0.0001$****. To justify the sample numbers in each group, a power analysis was performed based on the quantitative spectral results. Power values for each analysis was calculated using G*Power 3.[34]

3 Results and Discussions

The current study was conducted, for the first time, to explore the diagnostic potential of FTIR spectroscopy coupled with chemometrics in the differentiation of MPM from both LC and BPE groups. This spectroscopic method enables to elucidate the disease-induced global alterations in the biochemical makeup of cells, tissues, and even biofluids and thus discriminates the diseases from healthy conditions.[9,11,13,15,30,35,36] Although the FTIR microspectroscopy technique is more suitable for non-homogenous/homogenous liquid samples, in the current study, the ATR mode is preferred due to its easy use and relatively lower cost. ATR-FTIR spectroscopy has been proposed as an efficient useful diagnostic tool for a variety of diseases within the biomedical field toward translational medicine.[37,38]

In order to visually demonstrate the spectral differences between studied groups, the average spectra of MPM, LC, and BPE pleural fluids are shown in Fig. 1, in the 3800 to 800 cm^{-1} spectral region. As seen from this figure, the pleural fluid spectrum contains different vibrational modes of various functional groups belonging to various cellular constituents such as lipids, proteins, carbohydrates, and nucleic acids. The definition and assignment of these modes are indicated in Table 3. The spectra of the groups under study indicated that there are obvious differences in the constituents of MPM fluids, compared to the fluids from patients with LC and BPE (Fig. 1).

Based on their spectral differences, to test whether there is a differentiation between the groups under study, we first performed HCA to their IR spectra. Figures 2(a) and 2(b) show the HCA results of the MPM-LC and MPM-BPE groups, respectively, in the 3300 to 2800 cm^{-1} and 1800 to 650 cm^{-1} spectral regions. MPM was successfully differentiated from the BPE and LC fluids (Fig. 2). To measure the efficiency of this differentiation, we calculated the sensitivity and specificity based on the obtained cluster dendrograms. 100% sensitivity and 100% specificity were achieved in the differentiation of MPM and LC fluid samples, whereas 100% sensitivity and 88% specificity were obtained in the differentiation of MPM and BPE fluid samples. We also applied the same analysis to

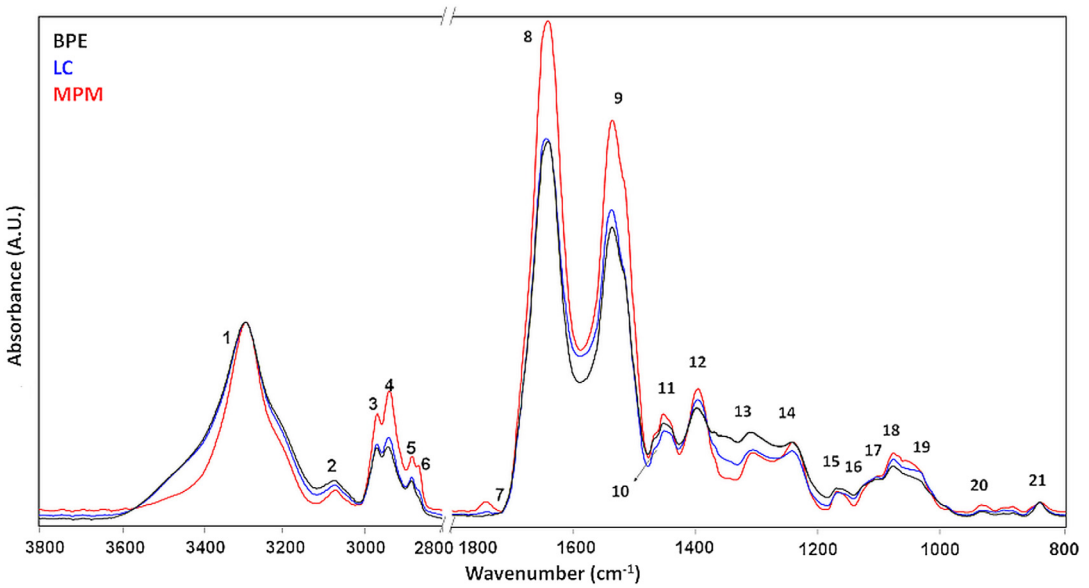

Fig. 1 The average FTIR absorption spectra of pleural fluid from BPE (black), LC (blue), and MPM (red) patients in the 3800 to 800 cm^{-1} spectral region. Min–max normalization process was performed based on amide A band.

Table 3 General band assignment of an ATR-FTIR spectrum of pleural fluid.

Band number	Band position (cm^{-1})	Definition	References
1	3286	Amide A: protein (N—H stretching)	39 and 40
2	3063	Amide B: protein	39
3	2959	CH_3 antisymmetric stretching: mainly lipid	41–43
4	2928	CH_2 antisymmetric stretching: mainly lipid	41–43
5	2871	CH_3 symmetric stretching:mainly protein	39 and 41
6	2852	CH_2 symmetric stretching: mainly lipid	41 and 42
7	1739	Ester C=O stretching:triglycerides and cholesterol esters	44
8	1643	Amide I: protein (80% C=O stretching, 10% N—H bending, 10% C—N stretching)	39
9	1537	Amide II: protein (60% N—H bending, 40% C—N stretching)	39
10	1470	CH_2 scissoring: lipid	45
11	1451	CH_3 antisymmetrich bending:protein	35
12	1397	COO^- symmetric stretching:fatty acids aminoacids	46
13	1308	Amid III: C—N stretching and ve N—H bending	47
14	1239	PO_2^- antisymmetric stretching: nucleic acids	48 and 49
15	1163	C—OH antisymmetric stretching: serine, tyrosine, threonine aminoacids of proteins	35
16	1123	C—O stretching: ribose	50
17	1104	P—O—P symmetric stretching: RNA	50 and 51
18	1076	PO_2^- symmetric stretching: nucleic acids and phospholipids	9
19	1030	C—O stretching and C—O bending carbohydrates	51 and 52
20	931	Z-form of DNA	53
21	836	DNA B-form helix conformation	54

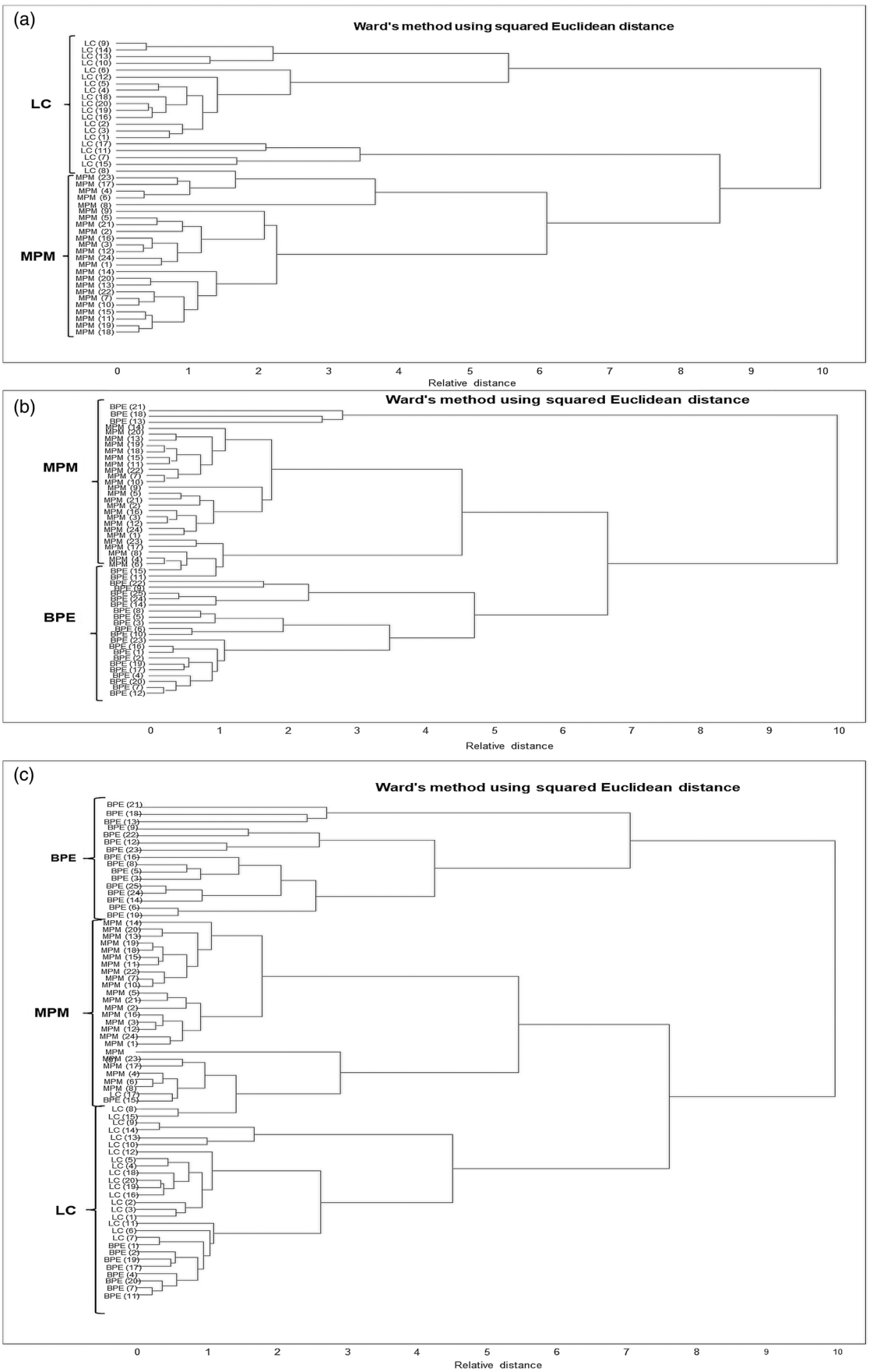

Fig. 2 HCA dendrograms of (a) MPM-LC, (b) MPM, BPE, and (c) MPM-LC-BPE groups in the 3300 to 2800 cm^{-1} and 1800 to 650 cm^{-1} spectral regions.

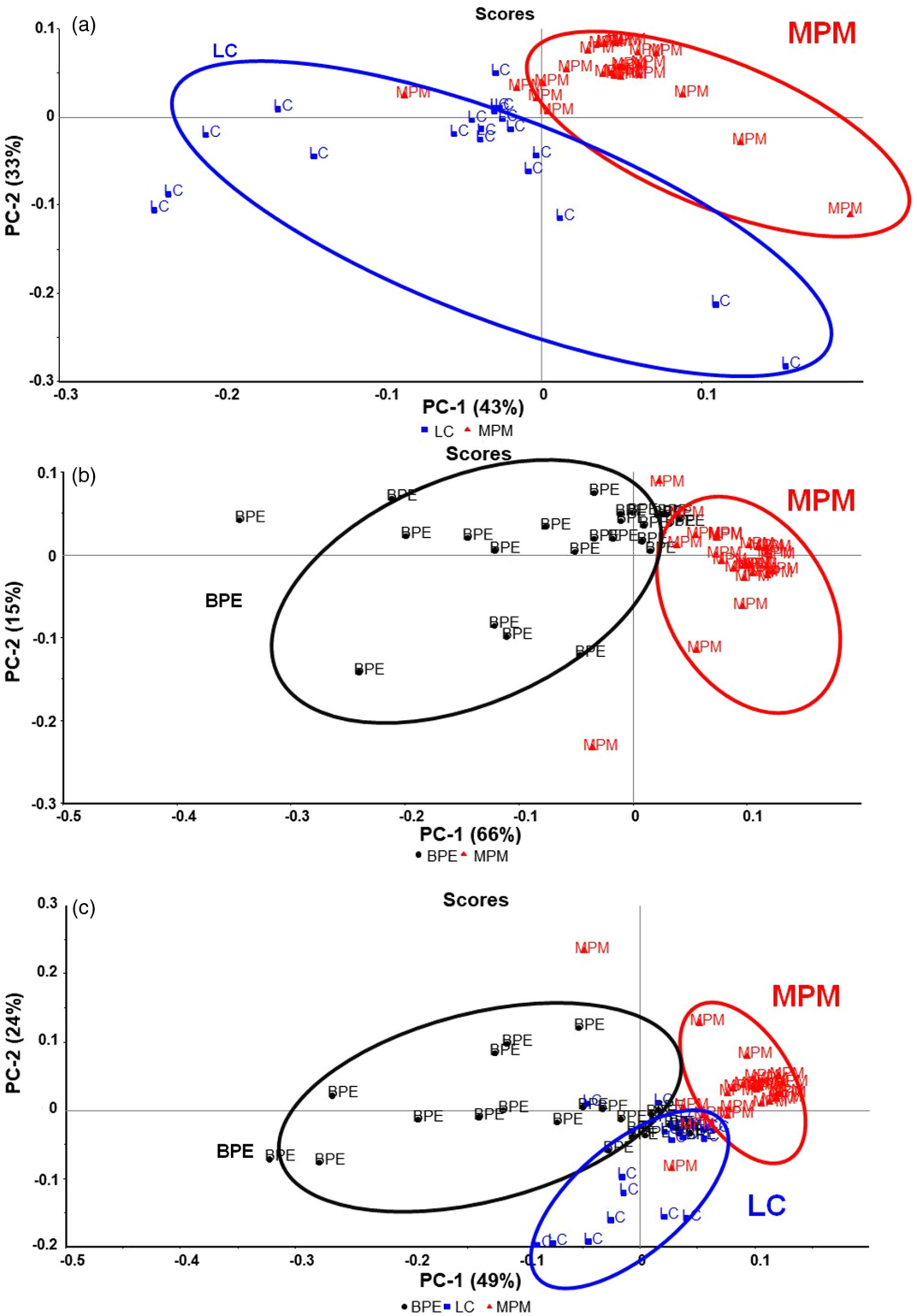

Fig. 3 PCA score plots of (a) MPM-LC, (b) MPM-BPE, and (c) MPM-LC-BPE groups in the 3300 to 2800 cm^{-1} and 1800 to 650 cm^{-1} spectral regions.

differentiate the three groups from each other, as shown in Fig. 2(c). Successful separation of these groups from each other with a high heterogeneity value was obtained.

To confirm the separation of the MPM, LC, and BPE groups from each other, PCA was also applied to their spectra in the 3300 to 2800 cm^{-1} and 1800 to 650 cm^{-1} spectral regions. Two dimensional scores plot of the first two PC for MPM-LC and MPM-BPE pairs are given in Figs. 3(a) and 3(b), respectively. Analysis of the scores plot for the MPM-LC pair demonstrated 43% of its variation to be accounted by the PC1

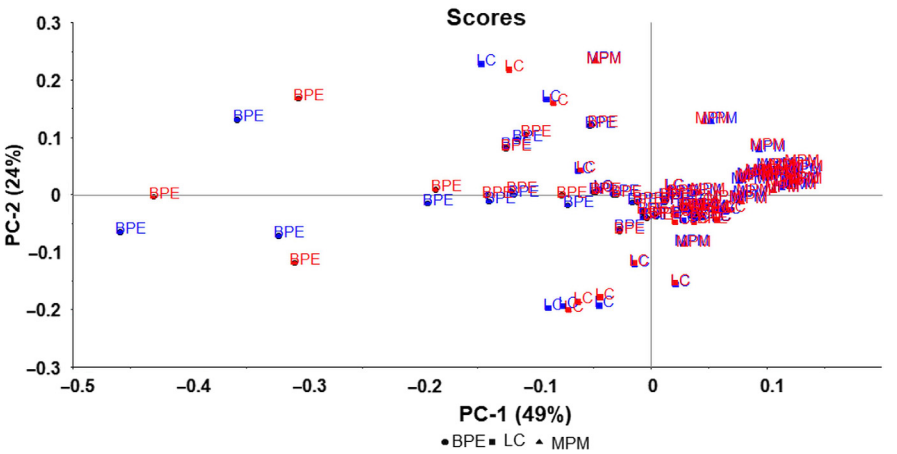

Fig. 4 PCA score plots for the whole 3300 to 2800 cm^{-1} and 1800 to 650 cm^{-1} spectral regions. The score plots for the calibration set (blue) and the scores for leave-one-out validation for each spectrum (red).

and 33% by the PC2. The same plot for the MPM-BPE pair showed that 66% of the variation was accounted by the PC1 and 15% by the PC2. These score plots clearly indicated the segregation of the MPM fluids from the LC and BPE fluids. PCA scores plot for MPM, LC, and BPE groups is shown in Fig. 3(c). Analysis of the scores plot for the whole region showed that 49% of the variation was accounted by the PC1 and 24% by the PC2. As can be seen from this figure, the MPM and LC fluids are well segregated from the BPE group and from each other. PCA score and loading plots were also obtained for the fingerprint and C—H regions (data not shown), indicating a clear separation between the groups with PC1 and PC2 in most cases. For all the PCAs performed in this work, full cross validation (i.e., leave-one-out validation) was used. The score plots obtained from the calibration set and the cross validation set were compared so that prediction errors are kept at a minimum level. Figure 4 shows the PCA result obtained from the calibration set (blue) and the scores corresponding to leave-one-out cross validation (red) for each sample. As seen from this figure, the calibration and cross validation results are very close to each other, and therefore, the PCA model obtained is reliable.

In order to identify that spectral bands contribute to the differentiation of MPM, LC, and BPE groups, we analyzed loading plots of PCA. The plots obtained for the analyzed spectral regions for MPM-LC, MPM-BPE, and MPM-LC-BPE groups are shown in Figs. 5(a)–5(c), respectively. They clearly exhibited that the spectral differences between the groups occurred most dramatically in the CH and fingerprint regions. The positive and negative peaks observed in the loading plots indicate that these peaks strongly affect the chemical composition of the sample at the particular band position. A high-positive score value for the corresponding loading plot indicates a positive contribution for the band position with high-positive peak while a negative contribution for a negative peak, and vice versa for a high-negative score value. The loading plots for MPM-LC pair demonstrated three positive peaks at 2956, 2924, and 2852 cm^{-1} in the CH region and one positive peak at 1655 cm^{-1} and two negative peaks at 1590 and 1387 cm^{-1} in the fingerprint region. Analysis of PC1 loading plot for MPM-BPE pair indicated that three positive peaks at 2958, 2928, and 2851 cm^{-1} were observed in the C—H region,

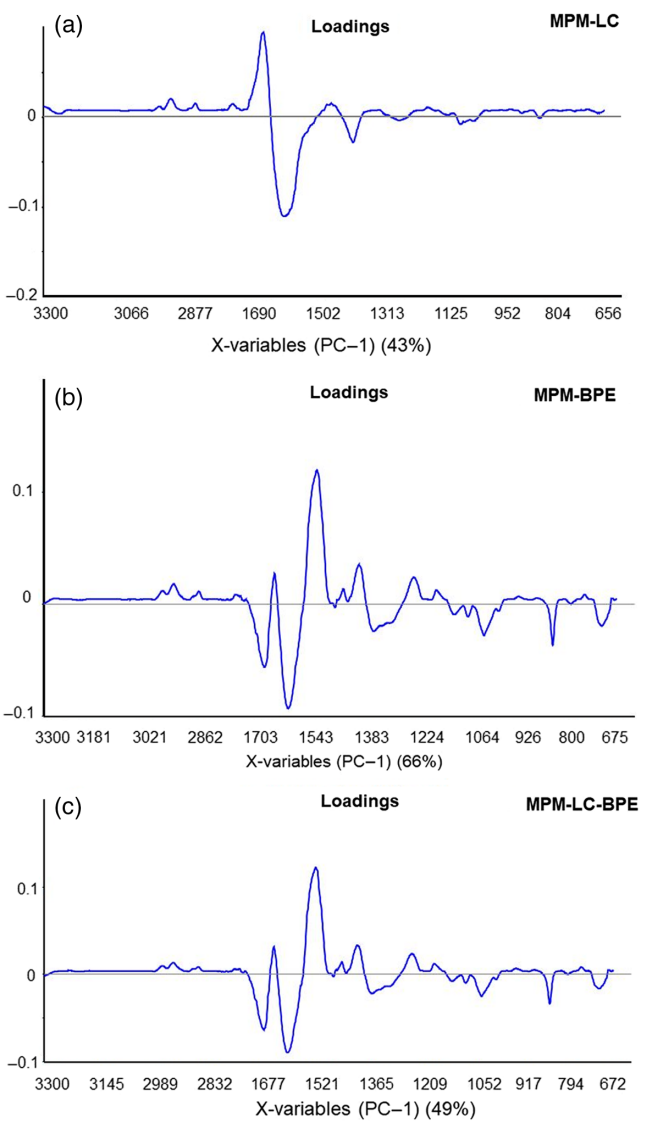

Fig. 5 PCA loading plots of (a) MPM-LC, (b) MPM-BPE, and (c) MPM-LC-BPE groups in the 3300 to 2800 cm^{-1} and 1800 to 650 cm^{-1} spectral regions.

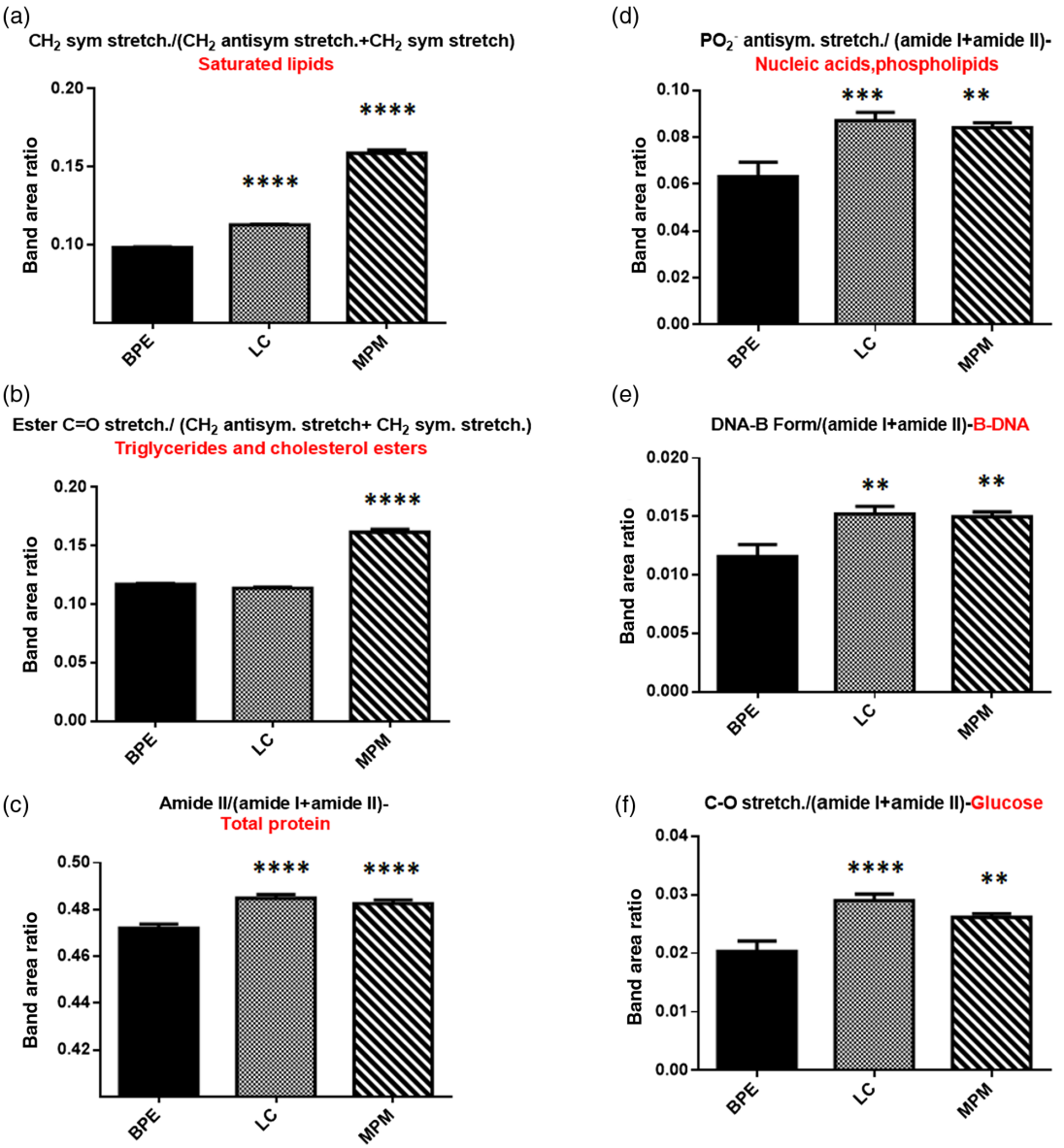

Fig. 6 (a) Band area ratio values of saturated lipids (3050 to 2800 cm^{-1}), (b) triglycerides and cholesterol ester (1800 to 650 cm^{-1}), (c) protein (1800 to 650 cm^{-1}), (d) nucleic acids and phospholipids (1800 to 650 cm^{-1}), (e) B-DNA (1800 to 650 cm^{-1}), and (f) glucose (1800 to 650 cm^{-1}) bands from the IR spectra of the MPM, LC, and BPE groups.

whereas negative peaks at 1666, 1595, 1118, 1077, 1030, and 834 cm^{-1} and positive peaks at 1435, 1389, 1230, and 1163 cm^{-1} were detected in the finger print region. The same plot for all three groups denoted positive peaks at 2958, 2928, and 2851 cm^{-1} for the C—H region and negative peaks at 1664 and 1593 cm^{-1} and positive peaks at 1436, 1395, 1236, and 1166 cm^{-1} in the fingerprint region. In these plots, the peaks observed at 2958, 2928, and 2851 cm^{-1} are attributed to lipids and fatty acids.[55,56] Moreover, the peaks seen at 1664 cm^{-1} are due to the α-helix structure of proteins. The peaks at 1395 and 1166 cm^{-1} originate from COO^- symmetric stretching of fatty acids and C—OH antisymmetric stretching of serine and tyrosine, respectively.[56–59]

To acquire the quantitative differences in these spectral peaks observed in the loading plots of the groups under study, spectral band area ratios for relevant peaks were calculated from their absorbance spectra. The band area ratio results of these peaks are shown in Fig. 6. The band area ratios of saturated lipids (CH_2 sym. stretch./CH_2 sym. Stretch + CH_2 antisym. stretch.), protein (amide II/amide I+amideII), B-DNA (DNA B form/ amide I + amide II), and glucose (C—O stretching/amide I + amide II) were found to be significantly higher for the MPM and LC groups with respect to the control group indicating that these spectral parameters can be used as biomarkers in cancer diagnosis. The band area ratio of the triglycerides and cholesterol ester (ester C═O stretching/amide I + amide II) was significantly higher only in the MPM groups with regards to the BPE group indicating that this spectral parameter can be used as a biomarker in the MPM diagnosis. The bandwidth and band position of the CH_2 antisymmetric stretching band were also analyzed whose results are shown in Figs. 7(a) and 7(b), respectively. The bandwidth values of this band for the MPM

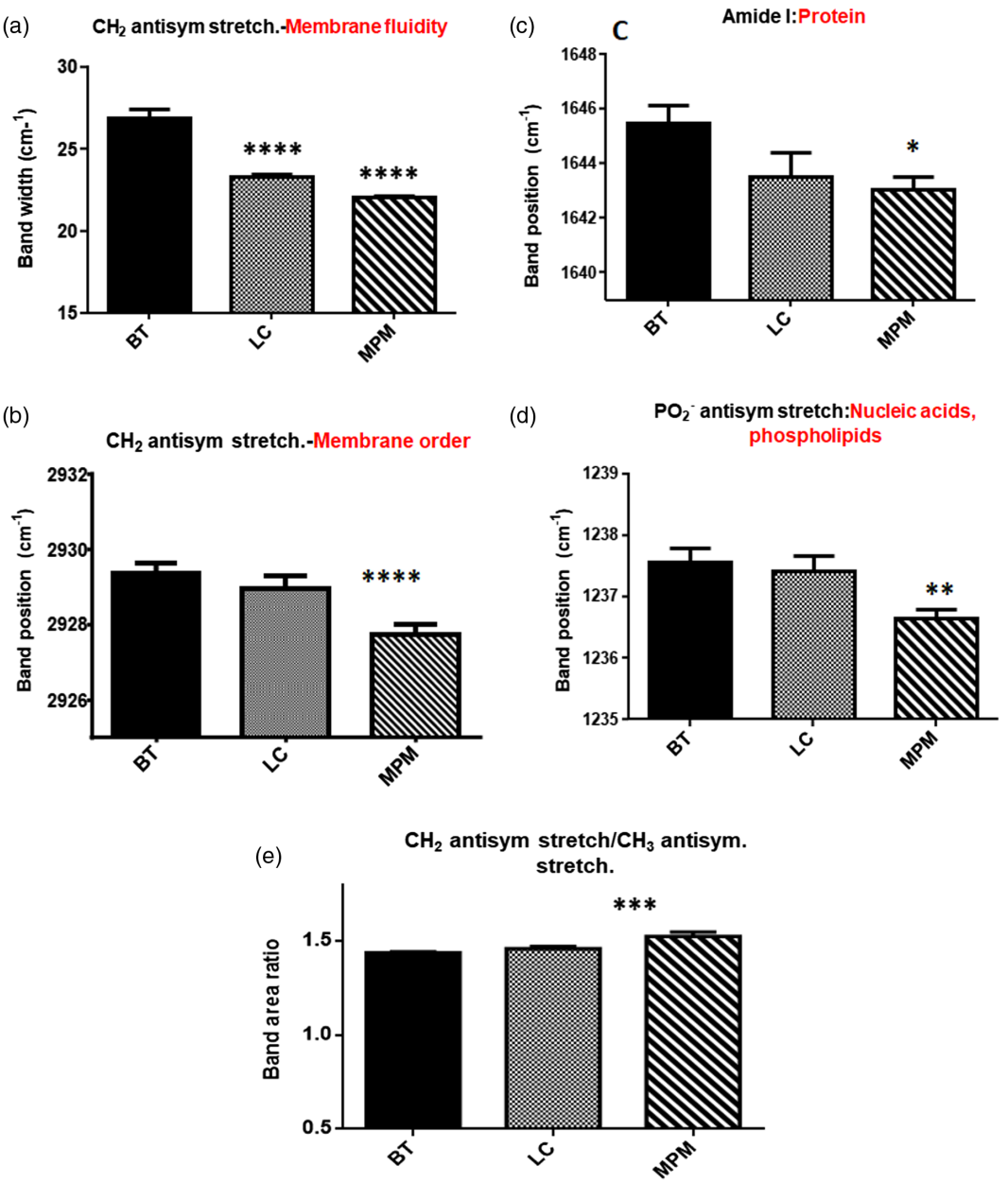

Fig. 7 (a) Bandwidth and (b) band position values of the CH_2 antisymmetric stretching band (3050 to 2800 cm^{-1}), (c) band position values of amide I, (d) PO_2^- antisymmetric stretching band (1800 to 650 cm^{-1}), and (e) band area ratio value of CH_2 antisymmetric/CH_3 antisymmetric stretching bands (3050 to 2800 cm^{-1}) from the IR spectra of the MPM, LC, and BPE groups.

and LC groups were observed to be significantly lower than that of the BPE group indicating that this spectral parameter can be specific biomarker to diagnose cancer. Moreover, a significant shift to lower values of the band position of the same band was found for the MPM group with respect to the BPE group, indicating that this spectral parameter can be used as a specific biomarker for the diagnosis of MPM. The band position analyses of amide I and PO_2^- antisymmetric stretching bands, which are demonstrated in Figs. 7(c) and 7(d), respectively, exhibited only a significant shift to lower values in the MPM group with respect to the BPE group. Figure 7(e) shows the changes in the band area ratio of CH_2/CH_3 antisymmetric stretching bands, indicating a significantly higher ratio only in the MPM group with respect to the BPE group. The results of Figs. 7(c)–7(e) also indicate that these spectral parameters can also be used as specific biomarkers for the diagnosis of MPM.

It is evident that in absorption spectroscopy, according to the Beer–Lambert law, an increase in the band area/intensity of a spectral band indicates an increased concentration of its respective functional group.[56] Therefore, the higher band area in the lipid, protein, and nucleic acid bands indicates a higher concentration of these molecules in MPM pleural fluid samples. Higher lipid content might be due to the higher lipid biosynthesis. This interpretation was supported by the higher band area ratio of the lipid related bands (CH_2 antisymmetric/CH_3 antisymmetric stretching), which indicates higher chain length in lipids, and thus elevated lipid synthesis.[60,61] This higher lipid synthesis in cancer cells arises from the need to compensate

their energy needs.[62,63] An increase in fatty acid synthase, the primary enzyme for the synthesis of fatty acids in MPM, was reported by Gabrielson et al.[64], confirming the elevated lipid synthesis and thus our results. Moreover, we have also found a higher triglyceride and cholesterol ester amount in the MPM pleural fluid group. Recently, Ravipati et al.[65] demonstrated the elevated plasma triglyceride level in lung cancer patients, which is in agreement with our results. Lower membrane fluidity and higher membrane order in the MPM group were also indicated from the lower bandwidth value and lower band position value of CH_2 antisymmetric stretching band. These alterations in membrane parameters can be associated with alterations in lipid composition, i.e., types of lipids and their relative concentrations, which affect the ion binding capacity of lipids, lipid membrane thickness, and lipid–lipid and lipid–protein interactions.[66,67] Moreover, the higher protein content in the MPM group may be associated with higher protein biosynthesis. The increment in this synthesis in cancer cells was demonstrated in recent studies.[68,69] Additionally, the increase in the soluble mesothelin related protein content in pleural fluid of mesothelioma patient has been previously reported in another study, supporting the reliability of our finding.[70] The higher protein content was also supported by the greater nucleic acid and B-DNA content in the MPM group. In addition to these findings, we also found conformational differences in the protein and nucleic acid structure of the MPM group as indicated by the shift in the band position values of the amide I (protein) and PO_2^- antisymmetric stretching (nucleic acid) bands.[71–73] Parallel to these results, changes in the protein secondary structure in colon cancer tissues was demonstrated by Chen et al.[74] Our finding related to the higher glycogen/glucose concentration in the MPM group was also supported by other studies, which demonstrated an alteration in glycogen content in mesothelioma patients. Based on all the compositional differences between the biomolecules of the MPM, LC, and BPE groups mentioned above, we can infer that these differences significantly contribute their differentiation from each other. Since our sample size is not very high, to be able to justify these differences between studied groups, we have performed power analysis for each quantitative spectral results. A range between 92% and 100% for power values were obtained, implying that sample size in each group are sufficient to draw conclusion about the obtained results. These findings also prove that IR spectroscopy coupled with chemometric approaches carries a promising diagnostic potential in MPM diagnosis. Therefore, to confirm this potential, we applied a PCA-based supervised classification technique, SIMCA, to the pleural fluid spectra of the studied samples in the 3300 to 2800 cm^{-1} and 1800 to 650 cm^{-1} spectral regions since it enables good classification of samples even with low sample size and high variability within-class.[75] To perform SIMCA analysis, three PCA models were developed from the spectra of the samples that make up the training data (BPE: 22, LC: 17, and MPM: 21). Figure 8(a) shows the distance of MPM and LC models to the BPE models, which was 8 and 16. The differentiation of the MPM group from the LC and BPE groups with a 5% significance level are also seen in the Cooman's plot presented in Figs. 8(b) and 8(c), respectively. In order to test our models, a test group was formed by randomly selecting three samples from each group, which were not included in the SIMCA training set. Then SIMCA analysis was performed to this test group. The selection and analysis process of samples were repeated 10 times and each time the percentage of correct classification of spectra was calculated. A correct classification ranges between 82% to 100% from 1st to 10th trials were obtained with an average percent value equal to 96.2% In SIMCA analysis, the model distance plot enables one to determine how different each model from each other with respect to PC space and thus the success of the classification method. A model distance >3 indicates that models are significantly different from each other. The high-distance values >3, as obtained in the model distance plot of the MPM, LC, and BPE groups, indicate a very robust and clear differentiation of both groups from the BPE fluids-group and from each other.[76–78] Moreover, Cooman's plot obtained from SIMCA analysis was also used to show the differentiation between two classes and the distance of test samples to their model. Cooman's plot of MPM versus LC and MPM versus BPE models demonstrated the correct classification of tested samples from each group with an average of 96.2% accuracy. It has been demonstrated that image-based diagnostic techniques for MPM including CT, positron emission tomography (PET), combination PET/CT, and MRI have a range of 88% to 94% sensitivity and 87% to 93% specificity.[79] Moreover, diagnostic studies based on marker identification from pleural fluids and serums indicate that the sensitivity of serum and pleural fluid soluble mesothelin-related proteins (SMPRs) are 61% and 79%, respectively, whereas their specificity are 87% and 85%, respectively.[80] Similar results from serum SMPRs have also been demonstrated by Luo et al.[81] In comparison to these results, in this study, higher sensitivity (100%) and specificity values (100% and 88%) for MPM diagnosis were obtained. Moreover, using the SIMCA method, a higher accuracy (96.2%) for the identification of MPM groups was acquired. With respect to the other diagnostic techniques for MPM diagnosis, our diagnostic approach, namely ATR-FTIR spectroscopy coupled with multivariate analysis, is a nondestructive, fast, reliable, relatively low-cost, operator-independent, and highly reproducible method.[82] Therefore, we propose that this approach has a promising potential for diagnosis with a higher accuracy.

4 Conclusion

In this study, high-throughput biomolecular profiling by FTIR spectroscopy with ATR mode revealed that the biomolecular composition and structure of pleural fluids of MPM samples differs from those of both LC and BPE pleural fluid samples. The characteristic biomolecular features of these fluids enable the differentiation of the all groups from each other, with several spectral findings that have diagnostic relevance. For example, we obtained dramatic changes in several spectral parameters such as lipid order, lipid dynamics, triglyceride, cholesterol ester concentration, and protein and nucleic acid structure, which are only specific to MPM patients. We obtained a very successful separation of MPM fluids from LC and BPE fluids with a high sensitivity and specificity as indicated by HCA and PCA. Moreover, we accurately identified test samples in each group by SIMCA analysis. We propose that compared to other conventional diagnostic techniques, FTIR spectroscopy coupled with multivariate analysis can improve and accelerate the diagnosis of MPM using pleural fluids in a label-free, rapid, robust, cost-effective, nondestructive, and reliable manner, in a time span of a few minutes. Moreover, this technical approach to diagnosis appears well suited for follow up and early diagnosis of high-risk groups, such as asbestos workers, carriers of germline BAP1 mutations, and individuals living in areas where

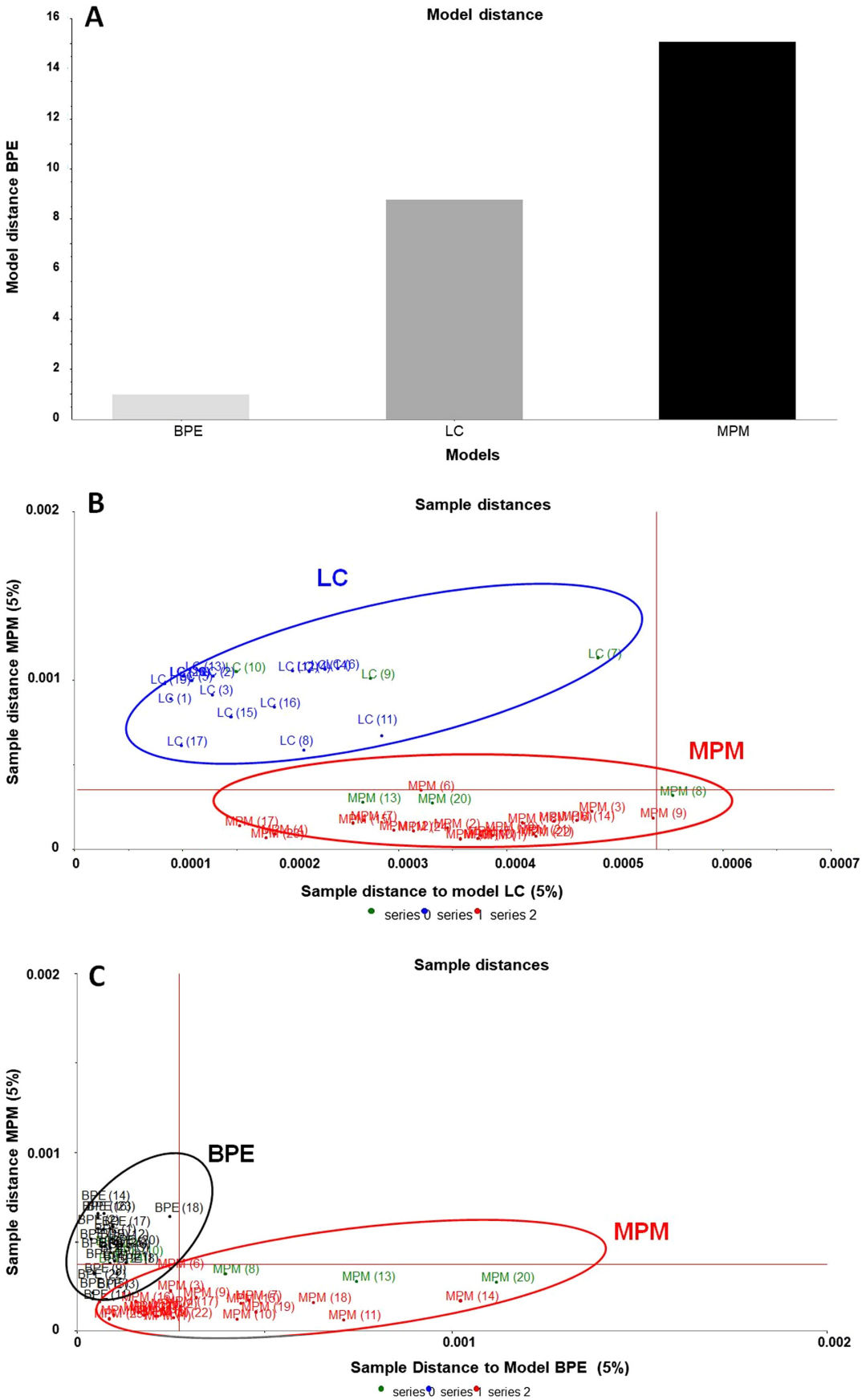

Fig. 8 (a) Distance in PCA space of MPM and LC calibration models from BPE model. Cooman's plot of (b) MPM (red)-LC (blue) groups and (c) MPM (red)-BPE (black) groups with test samples (green).

asbestos is present in the environment, such as in Turkey, North Dakota, and Nevada. When these individuals accumulate pleural fluids, FTIR spectroscopy coupled with multivariate analysis would provide a rapid and inexpensive method to rule out MPM or suggest the diagnosis of MPM that could then be confirmed by thoracoscopy and open biopsy without unnecessary delays.

Disclosures

The authors declare no conflict of interest.

Acknowledgments

This work was supported by the Health Sciences Research Group (SBAG) of the Scientific and Technological Research Council of Turkey (TUBITAK) (Project No: 113S294, 2013). The authors thank Dr. Sara Banu Akkas for her help with editing.

References

1. L. Mutti and V. C. Broaddus, "Malignant mesothelioma as both a challenge and an opportunity," *Oncogene* **23**(57), 9155–9161 (2004).
2. A. Napolitano et al., "HMGB1 and its hyperacetylated isoform are sensitive and specific serum biomarkers to detect asbestos exposure and to identify mesothelioma patients," *Clin. Cancer Res.* **22**(12), 3087–3096 (2016).
3. M. Carbone et al., "A mesothelioma epidemic in Cappadocia: scientific developments and unexpected social outcomes," *Nat. Rev. Cancer* **7**(2), 147–154 (2007).
4. M. A. Vaz et al., "Relationship between pleural fluid and serum cholesterol levels," *Chest* **119**(1), 204–210 (2001).
5. V. Delgermaa et al., "Global mesothelioma deaths reported to the World Health Organization between 1994 and 2008," *Bull. World Health Organ.* **89**(10), 716–724 (2011).
6. S. Jane Henley et al., "Mesothelioma incidence in 50 states and the District of Columbia, United States, 2003–2008," *Int. J. Occup. Environ. Med.* **19**(1), 1–10 (2013).
7. A. N. Husain et al., "Guidelines for pathologic diagnosis of malignant mesothelioma: a consensus statement from the International Mesothelioma Interest Group," *Arch. Pathol. Lab. Med.* **133**(8), 1317–1331 (2009).
8. M. Carbone et al., "Consensus Report of the 2015 Weinman international conference on mesothelioma," *J. Thorac. Oncol.* **11**(8), 1246–1262 (2016).
9. M. J. Baker et al., "FTIR-based spectroscopic analysis in the identification of clinically aggressive prostate cancer," *Br. J. Cancer* **99**(11), 1859–1866 (2008).
10. A. A. Bunaciu, V. D. Hoang, and H. Y. Aboul-Enein, "Applications of FT-IR spectrophotometry in cancer diagnostics," *Crit. Rev. Anal. Chem.* **45**(2), 156–165 (2015).
11. S. Gok et al., "Bladder cancer diagnosis from bladder wash by Fourier transform infrared spectroscopy as a novel test for tumor recurrence," *J. Biophotonics* **9**(9), 967–975 (2016).
12. P. D. Lewis et al., "Evaluation of FTIR spectroscopy as a diagnostic tool for lung cancer using sputum," *BMC Cancer* **10**(1), 640 (2010).
13. G. L. Owens et al., "Vibrational biospectroscopy coupled with multivariate analysis extracts potentially diagnostic features in blood plasma/serum of ovarian cancer patients," *J. Biophotonics* **7**(3–4), 200–209 (2014).
14. M. Verdonck et al., "Characterization of human breast cancer tissues by infrared imaging," *Analyst* **141**(2), 606–619 (2016).
15. X. Wang et al., "FTIR spectroscopic comparison of serum from lung cancer patients and healthy persons," *Spectrochim. Acta A Mol. Biomol. Spectrosc.* **122**, 193–197 (2014).
16. F. Großerueschkamp et al., "Spatial and molecular resolution of diffuse malignant mesothelioma heterogeneity by integrating label-free FTIR imaging, laser capture microdissection and proteomics," *Sci. Rep.* **7**, 44829 (2017).
17. S. Abbas et al., "Infrared spectroscopy as a novel approach in differential diagnosis of malignant pleural mesothelioma from lung cancer using pleural fluid," in *16th World Conf. on Lung Cancer (WLCL) 2015* (2015).
18. S. Abbas et al., "Evaluation of FTIR spectroscopy as a diagnostic tool for malignant pleural mesothelioma from pleural fluid," in *2nd Annual Int. Translational Nanomedicine Conf.*, Boston, USA (2014).
19. D. Yonar et al., "A novel method for early diagnosis of malignant pleural mesothelioma from human serum samples: ATR-FTIR spectroscopy," *Biophys. J.* **108**(2), 626a (2015).
20. G. Hoşafçı et al., "Clinical chemistry without reagents? An infrared spectroscopic technique for determination of clinically relevant constituents of body fluids," *Anal. Bioanal. Chem.* **387**(5), 1815–1822 (2007).
21. P. Lasch et al., "Antemortem identification of bovine spongiform encephalopathy from serum using infrared spectroscopy," *Anal. Chem.* **75**(23), 6673–6678 (2003).
22. M. Vives et al., "A study of Light's criteria and possible modifications for distinguishing exudative from transudative pleural effusions," *Chest* **109**(6), 1503–1507 (1996).
23. A. L. Mitchell et al., "Vibrational spectroscopy of biofluids for disease screening or diagnosis: translation from the laboratory to a clinical setting," *J. Biophotonics* **7**(3–4), 153–165 (2014).
24. E. Calabrò and S. Magazù, "The α-helix alignment of proteins in water solution toward a high-frequency electromagnetic field: a FTIR spectroscopy study," *Electromagn. Biol. Med.* **36**(3), 279–288 (2017).
25. L. Kerr and B. Hennelly, "A multivariate statistical investigation of background subtraction algorithms for Raman spectra of cytology samples recorded on glass slides," *Chemometr. Intell. Lab. Syst.* **158**, 61–68 (2016).
26. M. Kansiz, H. Billman-Jacobe, and D. McNaughton, "Quantitative determination of the biodegradable polymer poly (β-hydroxybutyrate) in a recombinant Escherichia coli strain by use of mid-infrared spectroscopy and multivariate statistics," *Appl. Environ. Microbiol* **66**(8), 3415–3420 (2000).
27. M. J. Baker et al., "Using Fourier transform IR spectroscopy to analyze biological materials," *Nat. Protoc.* **9**(8), 1771–1791 (2014).
28. H. Martens, J. P. Nielsen, and S. B. Engelsen, "Light scattering and light absorbance separated by extended multiplicative signal correction. Application to near-infrared transmission analysis of powder mixtures," *Anal. Chem.* **75**(3), 394–404 (2003).
29. C. Muehlethaler, G. Massonnet, and P. Esseiva, "Discrimination and classification of FTIR spectra of red, blue, and green spray paints using a multivariate statistical approach," *Forensic Sci. Int.* **244**, 170–178 (2014).
30. F. Severcan et al., "FT-IR spectroscopy in diagnosis of diabetes in rat animal model," *J. Biophotonics* **3**(8–9), 621–631 (2010).
31. H. H. Nieuwoudt et al., "Principal component analysis applied to Fourier transform infrared spectroscopy for the design of calibration sets for glycerol prediction models in wine and for the detection and classification of outlier samples," *J. Agric. Food Chem.* **52**(12), 3726–3735 (2004).
32. T. Nakamura et al., "Microspectroscopy of spectral biomarkers associated with human corneal stem cells," *Mol. Vision* **16**, 359 (2010).
33. D. Mueller et al., "Fourier transform infrared spectroscopy (FTIR) and multivariate analysis for identification of different vegetable oils used in biodiesel production," *Sensors* **13**(4), 4258–4271 (2013).
34. F. Faul et al., "G* Power 3: a flexible statistical power analysis program for the social, behavioral, and biomedical sciences," *Behav. Res. Methods* **39**(2), 175–191 (2007).
35. N. Fujioka et al., "Discrimination between normal and malignant human gastric tissues by Fourier transform infrared spectroscopy," *Cancer Detect. Prev.* **28**(1), 32–36 (2004).
36. E. Peuchant et al., "Infrared spectroscopy: a reagent-free method to distinguish Alzheimer's disease patients from normal-aging subjects," *Transl. Res.* **152**(3), 103–112 (2008).
37. K. Gajjar et al., "Diagnostic segregation of human brain tumours using Fourier-transform infrared and/or Raman spectroscopy coupled with discriminant analysis," *Anal. Methods* **5**(1), 89–102 (2013).
38. D. Yonar et al., "Relapsing-remitting multiple sclerosis diagnosis from cerebrospinal fluids via Fourier transform infrared spectroscopy coupled with multivariate analysis," *Sci. Rep.* **8**(1), 1025 (2018).

39. A. Barth, "Infrared spectroscopy of proteins," *Biochim. Biophys. Acta Bioenergy* **1767**(9), 1073–1101 (2007).
40. M. Jackson and H. H. Mantsch, "The use and misuse of FTIR spectroscopy in the determination of protein structure," *Crit. Rev. Biochem. Mol. Biol.* **30**(2), 95–120 (1995).
41. Y. Zhang et al., "Changes in attenuated total reflection Fourier transform infrared spectra as blood dries out," *J. Forensic Sci.* **62**(3), 761–767 (2017).
42. L. Di Giambattista et al., "New marker of tumor cell death revealed by ATR-FTIR spectroscopy," *Anal. Bioanal. Chem.* **399**(8), 2771–2778 (2011).
43. E. Giorgini et al., "FTIR microspectroscopic characterization of Spitz nevi," *Spectrochim Acta A Mol. Biomol. Spectros.* **141**, 99–103 (2015).
44. M. Nara, M. Okazaki, and H. Kagi, "Infrared study of human serum very-low-density and low-density lipoproteins. Implication of esterified lipid C=O stretching bands for characterizing lipoproteins," *Chem. Phys. Lipids* **117**(1), 1–6 (2002).
45. M. Boncheva, F. Damien, and V. Normand, "Molecular organization of the lipid matrix in intact Stratum corneum using ATR-FTIR spectroscopy," *Biochim. Biophys. Acta* **1778**(5), 1344–1355 (2008).
46. R. Gautam et al., "Molecular profiling of sepsis in mice using Fourier transform infrared microspectroscopy," *J. Biophotonics* **9**(1–2), 67–82 (2016).
47. L. Chiriboga et al., "Infrared spectroscopy of human tissue. I. Differentiation and maturation of epithelial cells in the human cervix," *Biospectroscopy* **4**(1), 47–53 (1998).
48. B. Rigas and P. T. Wong, "Human colon adenocarcinoma cell lines display infrared spectroscopic features of malignant colon tissues," *Cancer Res.* **52**(1), 84–88 (1992).
49. A. Pevsner and M. Diem, "Infrared spectroscopic studies of major cellular components. Part II: the effect of hydration on the spectra of nucleic acids," *Appl. Spectrosc.* **55**(11), 1502–1505 (2001).
50. A. Heidari, "An analytical and computational infrared spectroscopic review of vibrational modes in nucleic acids," *Austin J. Anal. Pharm. Chem.* **3**(1), 1058 (2016).
51. Z. Movasaghi, S. Rehman, and D. I. ur Rehman, "Fourier transform infrared (FTIR) spectroscopy of biological tissues," *Appl. Spectrosc. Rev.* **43**(2), 134–179 (2008).
52. G. J. Vazquez-Zapien et al., "FTIR spectroscopic and molecular analysis during differentiation of pluripotent stem cells to pancreatic cells," *Stem cells Int.* **2016**, 1–10 (2016).
53. M. K. Ahmed, F. Amiama, and E. A. Sealy, "Unique spectral features of DNA infrared bands of some microorganisms," *J. Spectrosc.* **23**(5–6), 291–297 (2009).
54. E. Taillandier and J. Liquier, "[16] Infrared spectroscopy of DNA," in *Methods in Enzymology*, D. Lilley and J. Dahlberg, Eds., pp. 307–335, Elsevier (1992).
55. F. Bonnier, M. J. Baker, and H. J. Byrne, "Vibrational spectroscopic analysis of body fluids: avoiding molecular contamination using centrifugal filtration," *Anal. Methods* **6**(14), 5155–5160 (2014).
56. F. Severcan and P. I. Haris, *Vibrational Spectroscopy in Diagnosis and Screening*, IOS Press, Amsterdam (2012).
57. M. Correia et al., "FTIR spectroscopy—a potential tool to identify metabolic changes in dementia patients," *J. Alzheimers Neurodegener.* **2**(2), 007 (2016).
58. R. Lu et al., "Probing the secondary structure of bovine serum albumin during heat-induced denaturation using mid-infrared fiberoptic sensors," *Analyst* **140**(3), 765–770 (2015).
59. A. Sevinc, D. Yonar, and F. Severcan, "Investigation of neurodegenerative diseases from body fluid samples using Fourier transform infrared spectroscopy," *Biomed. Spectrosc. Imaging* **4**(4), 341–357 (2015).
60. F. K. Baloglu et al., "FTIR imaging of structural changes in visceral and subcutaneous adiposity and brown to white adipocyte transdifferentiation," *Analyst* **140**(7), 2205–2214 (2015).
61. R. N. Lewis and R. N. McElhaney, "Membrane lipid phase transitions and phase organization studied by Fourier transform infrared spectroscopy," *Biochim. Biophys. Acta* **1828**(10), 2347–2358 (2013).
62. F. Baenke et al., "Hooked on fat: the role of lipid synthesis in cancer metabolism and tumour development," *Dis. Model Mech.* **6**(6), 1353–1363 (2013).
63. J. A. Menendez and R. Lupu, "Fatty acid synthase and the lipogenic phenotype in cancer pathogenesis," *Nat. Rev. Cancer* **7**(10), 763–777 (2007).
64. E. W. Gabrielson et al., "Increased fatty acid synthase is a therapeutic target in mesothelioma," *Clin. Cancer Res.* **7**(1), 153–157 (2001).
65. S. Ravipati et al., "Plasma lipid biomarker signatures in squamous carcinoma and adenocarcinoma lung cancer patients," *Metabolomics* **11**(6), 1600–1611 (2015).
66. M. Inbar et al., "Fluidity difference of membrane lipids in human normal and leukemic lymphocytes as controlled by serum components," *Cancer Res.* **37**(9), 3037–3041 (1977).
67. P. V. Escriba et al., "Membranes: a meeting point for lipids, proteins and therapies," *J. Cell. Mol. Med.* **12**(3), 829–875 (2008).
68. S. C. Dolfi et al., "The metabolic demands of cancer cells are coupled to their size and protein synthesis rates," *Cancer Metab.* **1**(1), 20 (2013).
69. D. Silvera, S. C. Formenti, and R. J. Schneider, "Translational control in cancer," *Nat. Rev. Cancer* **10**(4), 254–266 (2010).
70. B. W. Robinson et al., "Mesothelin-family proteins and diagnosis of mesothelioma," *Lancet* **362**(9396), 1612–1616 (2003).
71. J. Wang and M. A. El-Sayed, "Temperature jump-induced secondary structural change of the membrane protein bacteriorhodopsin in the premelting temperature region: a nanosecond time-resolved Fourier transform infrared study," *Biophys. J.* **76**(5), 2777–2783 (1999).
72. P. I. Haris, G. Molle, and H. Duclohier, "Conformational changes in alamethicin associated with substitution of its α-methylalanines with leucines: a FTIR spectroscopic analysis and correlation with channel kinetics," *Biophys. J.* **86**(1), 248–253 (2004).
73. G. Dovbeshko et al., "Gold and colloidal gold surface influence on DNA conformational change," *Semicond. Phys. Quantum Electron. Optoelectron.* **7**(3), 318–325 (2004).
74. Y. Chen et al., "Study on the secondary structure of protein in amide I band from human colon cancer tissue by Fourier-transform infrared spectroscopy," *Chang Gung Med. J.* **24**(9), 541–546 (2001).
75. M. Bylesjö et al., "OPLS discriminant analysis: combining the strengths of PLS-DA and SIMCA classification," *J. Chemometrics* **20**(8–10), 341–351 (2006).
76. A. K. Myakalwar et al., "Laser-induced breakdown spectroscopy-based investigation and classification of pharmaceutical tablets using multivariate chemometric analysis," *Talanta* **87**, 53–59 (2011).
77. O. A. Coubard, "A method for processing multivariate data in medical studies," *Stat. Med.* **32**(20), 3436–3448 (2013).
78. R. Bro and A. K. Smilde, "Principal component analysis," *Anal. Methods* **6**(9), 2812–2831 (2014).
79. I. Zahid et al., "What is the best way to diagnose and stage malignant pleural mesothelioma?" *Interact. Cardiov. Thorac. Surg.* **12**(2), 254–259 (2011).
80. A. Cui et al., "Diagnostic values of soluble mesothelin-related peptides for malignant pleural mesothelioma: updated meta-analysis," *BMJ open* **4**(2), e004145 (2014).
81. L. Luo et al., "Diagnostic value of soluble mesothelin-related peptides for malignant mesothelioma: a meta-analysis," *Resp. Med.* **104**(1), 149–156 (2010).
82. S. Lagniau et al., "Biomarkers for early diagnosis of malignant mesothelioma: do we need another moonshot?" *Oncotarget* **8**(32), 53751 (2017).

Sherif Abbas received his MSc degree in biophysics from Ain Shams University, Egypt, in 2007. In his MSc study, he worked on medical image analysis of white blood cells. His PhD study focused on the investigation of protein structure and dynamics using spectroscopic techniques and artificial neural networks. His main research interests are molecular biophysics, spectroscopy, ANNs, and medical signal and image analysis.

Nihal Simsek Ozek studied biology at Ankara University, Turkey. She received her MSc degree in biology from the Middle East Technical University (METU) in 2007, related to toxic effects of statins and her PhD in biology from METU in 2015, related to microRNA and breast cancers. Currently, she is working as a PhD research assistant in the Department of Biology at Ataturk University. Her main interests are drug toxicities, spectroscopy, cancer genetics, and medical diagnostics.

Salih Emri graduated from the School of Medicine in Hacettepe University in 1982, and worked as a lecturer and professor for at least 30 years in the Department of Pulmonology until 2016. He

holds a full professor position in the Department of Pulmonology, Altinbas University, Istanbul, since that year. He is currently working in Medical Park Goztepe Hospital in Istanbul. His main interests are environmental and occupational chest diseases, tobacco control, and thoracic malignancies.

Deniz Koksal graduated from Hacettepe University, School of Medicine in 1996 and completed her residency training on pulmonology in the Department of Chest Diseases at Ankara University School of Medicine. She is working as a professor in the Department of Chest Disease of Hacettepe University Hospital. Currently, she is a member of administrative board of Pleura Study Group of Turkish Respiratory Research Society. She has many publications in the era of pulmonary medicine.

Mete Severcan received his BSc and MSc degrees from METU in 1968 and 1970 and his PhD from Stanford University in 1974. Since then, he has been a member of the Department of Electrical Engineering of METU and worked as a consultant in industry. His research interests are telecommunications, image and signal processing, and application of signal processing and bioinformatics techniques to FTIR signals for disease diagnosis, and characterization of biological systems.

Feride Severcan received her BSc degree from Ankara University, her MSc degree from Rochester University, and her PhD from Hacettepe University all in physics. She did postdoctoral study in Stanford and San Francisco State Universities and worked as a research associate at Perugia University. She was a professor of Biological Science Department of METU, between 1992 and 2106. She is now a member in the Department of Biophysics at Altinbas University. Her main interests are biological spectroscopy, medical diagnostics, drug-biological system interactions, and ecotoxicology.